STUDY OF NEW CALIBRATION TECHNIQUES AND APPLICATIONS FOR PALSAR POLARIMETRIC MODE

PI No 102

Alexander Zakharov

FIRE RAS, Vvedensky square 1, Fryazino, 141190 Moscow region, Russia,

1. INTRODUCTION

The variety of PALSAR operation modes provides unique opportunities in the area of Earth remote sensing, though complicates at the same time radiometric calibration. The main idea of our proposal was to demonstrate new thematic applications of PALSAR data as well as to conduct study of new techniques of PALSAR radiometric and polarimetric calibration by means of passive targets – large parabolic antennas and natural persistent scatterers.

2. RESEARCH IMPLEMENTATION

2.1. Calibration studies

Two test sites were selected for PALSAR calibration studies – Bear Lakes test site in Moscow region and Istomino plus Ivolga/Khurumsha test site near Baikal Lake in Siberia. For the PALSAR calibration activities in Moscow region we proposed firstly to use 3 parabolic antennas 4.7 meters in diameter with 50 m spacing between the antennas. The antennas are reconstructed by means of the insertion of various scatterers (conducting disks and diffraction grid) in the focal area. The scattering properties of such passive calibration targets were widely examined with a use of ERS SAR in 1999-2006 under AO3-343 project. The antennas demonstrated very high ~ 59 dBm^2 and stable ~ 0.1 dB cross section in C-band. As it was shown in the special sub series of experiments, the antenna pattern after the insertion of the disc become relatively wide ~10^0, what allows to decrease the requirements to the pointing accuracy of calibration antennas. From experience gained we can conclude, that these antennas with disc and polarization grid are most interesting targets for PALSAR calibration.

An extensive series of calibration experiments of PALSAR with Bear Lakes antennas were conducted firstly in 2006 under Cal/Val activity. The antennas demonstrated high ~ 43 dBm^2 RCS, though because of narrow patterns some of SAR sessions were not successful; also because of mixture of PALSAR observation modes used the stability was not high enough. On the Fig. 1 the RCS of 3 calibration targets, 3 antennas, is presented. Target 2 is antenna with diffraction grid in focal area having 45^0 orientation angle of the grid relative to horizon. For that reason the backscatter of given antenna was approximately 6 dB lower than that of antennas with conducting disc.

To demonstrate long term PALSAR radiometric stability we selected about 50 observations of Bear Lakes calibration site made in FBS34.3 and FBD34.3 modes from tracks 585 and 586. We discovered that the antennas demonstrated relatively high ~ 43 dBm^2 RCS with remarkable stability. A subset of 37 measurements made for observations with correct antennas pointing in FBS 34.3 and FBD34.3 modes is presented on a Fig. 2.

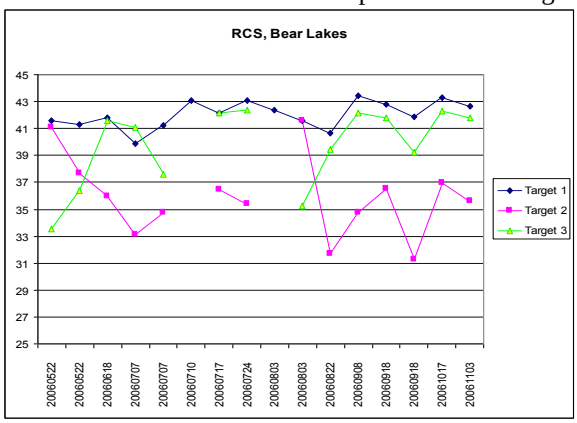

Fig. 1 RCS of 3 calibration antennas in 2006 according to 16 PALSAR observations.

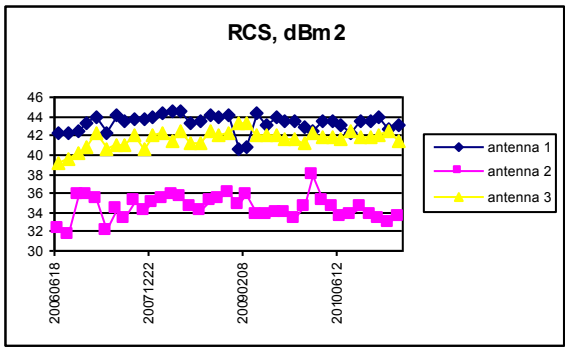

Fig. 2 RCS of 3 calibration antennas in 2006-2010 according to 37 PALSAR observations.

We can see here that the RCS stability of antenna 1 is higher than antennas 2 and 3 because of its wider pattern and affect of the pointing errors of latter ones. If we remove 2 observations made in severe winter 2009 conditions from entire dataset, we get for antenna 1 RCS 43.43 dBm^2 with standard deviation 0.64 dB. Antenna 3 (with 0.5 disk in focal area) has RCS 41.5 dBm^2 with standard deviation 0.86 dB. Antenna 2 with diffraction grid oriented at 45^0 respective to horizon has RCS 34.4 dBm^2 with 1.2 dB deviation.

As the antennas instability in L-band was found to be much larger than in C-band, it was decided to resolve the question by using some other reference targets - strong natural scatterers as potentially stable scatterers. A special procedure was invented to select them. More than 15 strong point targets near the calibration site were selected as candidates for our calibration

experiment with natural targets. As most of the strong backscattering signals are likely to be generated by dihedral structures on the surface (buildings, etc) having narrow scattering pattern, the selection of repeated orbits observations was made consciously.

In spite of the fact all the targets selected seem to be visually permanently bright on the images, the RCS fluctuations of most natural targets appeared to be unacceptable for our study. Some of targets revealed seasonal and some others - annual variations of their RCS. All the targets with more than 5 dB variations of RCS were excluded from consideration. The result for 2 most stable natural targets from a subset of 48 scenes being selected is plotted on a Fig. 3 below. In a contrast with reflector antennas, which were not identified in all the sessions, the natural targets selected could be seen on all 48 images.

As it can be seen, one of natural targets (target 2) demonstrates unique scattering stability. According to its statistics, it has RCS to be 45.4 dBm^2 with 0.54 dB standard deviation. For a subset of 21 observations made from track 585 we got 0.53 dB standard deviation and for a subset of 26 observations made from track 586 we got 0.54 dB on more than 4 years interval of PALSAR operation. Our analysis of measurements series made from different tracks (not seen on Fig. 3) shows that there is some indication of systematic underestimation of the RCS during last two years.

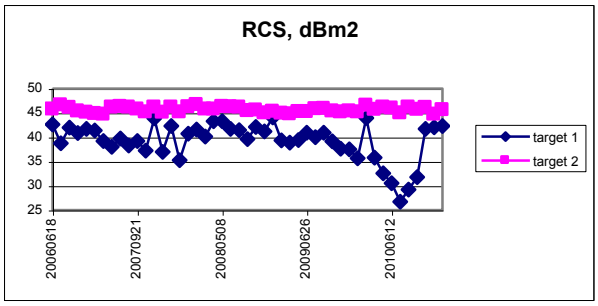

Fig. 3 RCS of 2 natural stable scatterers in 2006-2010 according to 48 PALSAR observations

Calibration site in Siberia was involved also into Cal/Val calibration activities in 2006. Two calibration sites were used: in Istomino settlement (Selenga river delta, Baikal Lake coastal area) and Ivolga (150 km to the South from Baikal). 6 corner reflectors with 2 m leg and triangular plates having 31 dBm^2 in L-band were placed at these test sites. Cal/Val activities confirmed their theoretical RCS values, though the measurements dispersion was too large because of deficient level of backscatter compared with clutter. Only Istomino corners were reliably observable on PALSAR images (not in all the observation modes). In 2007 the calibration observations of Istomino test site were continued. Mean RCS is 30.6 dBm^2 and close to theoretical one. The dispersion of measurements was too large again to be considered as indication of instability of PALSAR system. Most probable explanation is that 2 m leg size of corner is not enough for L-band SAR with a resolution of 5-10 m. Some results of Istomino corners RCS measurements from 27 PALSAR observations are plotted on Fig. 4.

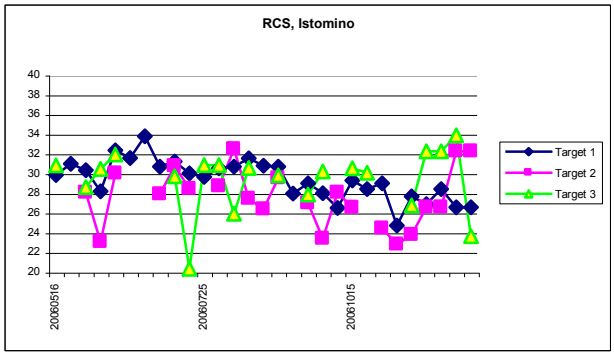

Fig. 4 RCS of 3 Istomino corner reflectors in 2006-2007according to 27 PALSAR observations

An enlarged corner reflector with 2.5 leg established in Ivolga test site in Siberia also demonstrated large RCS instability (see Fig. 5).

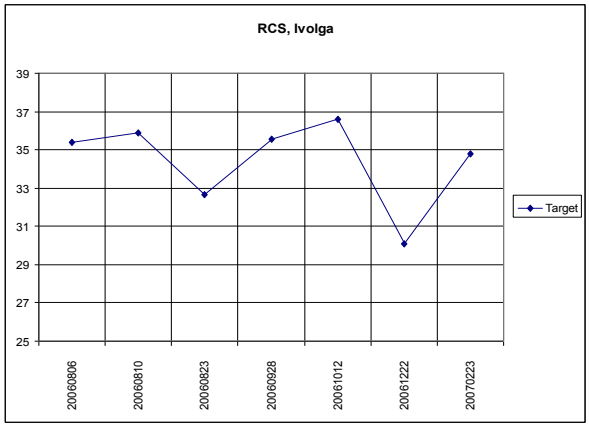

Fig. 5 RCS of Ivolga corner reflector in 2006-2007according to 7 PALSAR observations

An attempt to use bright natural scatterers in rural area of Istomino -power line towers - was unsuccessful as the variations of towers backscatter were too high.

Polarimetric calibration with 3 Bear Lakes calibration targets was not successful as the targets matrices do not fit the respective requirements for their scattering matrices, but some of receive/transmit elements of distortion matrices could be determined.

If ***D*** is scattering matrix of antenna with disk and ***G*** is scattering matrix of antenna with diffraction grid, then receive and transmit channel imbalances are

$$f_r \approx \sqrt{\frac{\frac{D_{hv}}{D_{hh}} - \frac{G_{hv}}{G_{hh}}}{\frac{D_{vh}}{D_{hh}} - \frac{G_{vh}}{G_{hh}}} \frac{D_{vv}}{D_{hh}}}$$

$$f_t \approx \frac{\frac{D_{vv}}{D_{hh}}}{\sqrt{\frac{\frac{D_{hv}}{D_{hh}} - \frac{G_{hv}}{G_{hh}}}{\frac{D_{vh}}{D_{hh}} - \frac{G_{vh}}{G_{hh}}} \frac{D_{vv}}{D_{hh}}}}$$

Using PALSAR measurements we got f_r= 0.733-j0.004 (JAXA value 0.722-j0.0237) and f_t=0.973+j0.365 (JAXA value 0.957+j0.383). Transmit/receive crosstalks were estimated using Quegan algorithm in the case of low TEC and Faraday rotation values:

t12=0.0042-j0.011 (JAXA value 0.024+j0.013),
t21=-0.036+j0.004 (JAXA value -0.011-j0.006),
r12=0.0092+j0.004 (JAXA value -0.006+j0.007),
r21=-0.009-j0.0062 (JAXA value –0.0063+j0.008).

3.2. Thematic analysis with PALSAR data then

3.2.1. Forests studies

Full-polarimetric interferometric data allows introducing the vector coherence, which uses an ensemble of pairs of scattering matrices. For this type of data one can calculate a conventional coherence map for any combination of polarizations on receive/transmit for both images.

We present here novel method of vector coherence visualization, which illustrates both interferometric and polarimetric sides of POLINSAR data. The central idea of the method is the following. One can associate each pixel of the co-registered images (or, rather, a set of pixels with a given pixel in the center of it) with a plot of the coherence magnitude as a function of orientation and ellipticity angles. By analogy with standard terminology of polarimetric SAR, we name this plot "a polarimetric coherence signature".

For the purpose of classification the following observation is of grate importance: coherence signatures have a similar shape for the same type of cover, and different types of cover show different signatures. The term "shape" means here the positional relationship of global and local maxima and minima in the plot. As in the case of conventional polarization signatures, where radar cross section is the function of polarization ellipse parameters, analysis of a coherence signature shape gives an additional information on the scattering surface.

Before implementing classification based on the coherence signatures, it is interesting to analyze some common properties of the signatures. Let us concentrate on co-polar signatures.

At first sight the shape of a coherence signature and of a conventional polarization signature are similar to each other. As a rule, the "linear polarization" profile (with zero ellipticity angle) dominates for land covers of different types, and circular polarization sides of the plot (ellipticity is equal to +45° and –45°) are down. Maxima and minima of the linear polarization profile usually correspond to the vertical polarization (orientation angle is equal to 90°) and/or the horizontal one (orientation angle is 0° or 180°).

The experimental data used in this study are full-polarimetric ALOS PALSAR repeat-pass scenes covering areas near calibration sites mentioned above: southeastern shore of Baikal Lake, Siberia, and Bear Lakes near Moscow.

Coherence signatures for forest can be divided into three sub-types: with global maximum localized at horizontal linear polarization and with two local maxima at horizontal and vertical at linear polarizations. In the case of processing large areas (the whole forest, for example) we get the first type of signature. After discussion of possible sources of signal decorrelation the temporal decorrelation looks like the main factor. Thus, this shape of coherence signature shows the prevailing stability of horizontally oriented scatterers. Analysis of smaller parts of images adds the second type of coherence signature shape, where we can see high temporal stability of vertically oriented scatterers also. The level of the second maximum can be both less or greater than the first one, supposedly according to the contribution of the correspondent orientation of elementary scatterers in the temporal decorrelation.

Non-forested lands (field, meadows, etc.) introduce another type of coherence signatures. The main feature of this type of signatures is the absence of point maximum but the presence of the maximal line at the linear polarization (with zero ellipticity angle). For other values of ellipticity angle the magnitude of the coherence does not depend on the orientation angle, too. So we can say that there is no selected orientation of elementary scatterers for this type of cover that indicates a surface scattering. The decrease of coherence magnitude from linear to circular polarization can be explained by reduction of cross-section value for circular polarization. Sometimes one can see slight maximum in the field-like signatures at the vertical linear polarization. A feature can appear due to seasonal growth of vegetation, what is natural for 46-days revisit period.

Water surfaces show the total decorrelation in the repeat-pass interferogram, and chaotic coherence signature.

Coherence signatures of urban areas were examined only for Bear Lakes test site. Coherence signatures for this type of cover are of special shape. The maximum at horizontal polarization is similar to forest coherence signatures. But at the vertical linear polarization values of coherence magnitude are greater than for the case of forests. Generally, this type of signatures looks like combination of field-like signature and forest-like one. Forest-like component is supposed to correspond to greenery, and the field-like component with surface type of scattering should be an impact of flat surfaces (squares, wide roofs, broad avenues).

Coherence signatures analysis can be integrated with examination of coherence regions in the unit circle for the same areas. Four above-mentioned types of cover one can draw a coherence region that deals also with phase information. The brief description of coherence regions: fields show higher radial and phase diversity than other types of cover. Coherence regions for forests in general are very compact.

There are two types of forest coherence regions in our data: near-circular and oblique. The latter are suitable for some POLINSAR methods that uses linear model of coherence. But about 40% of our forest coherence regions were not oblique. Coherence regions for urban areas are near-linear, especially for cross-polar values. Finally, water surface coherence regions have an unpredictable irregular form and always include zero as a result of total decorrelation.

An example of coherence signature (co-pol and cross-pol) is presented on the figures below. Such a coherence signatures may be used for classification in a form of a comparison the observed signatures with template ones according to some likelihood criteria.

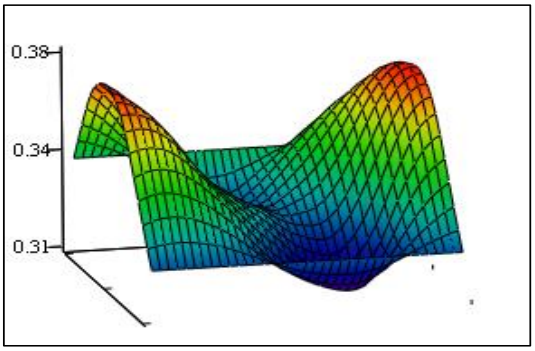

m

Fig. 6 Example of co-pol coherence signature for forest in Bear Lakes area for 20060822-20061007

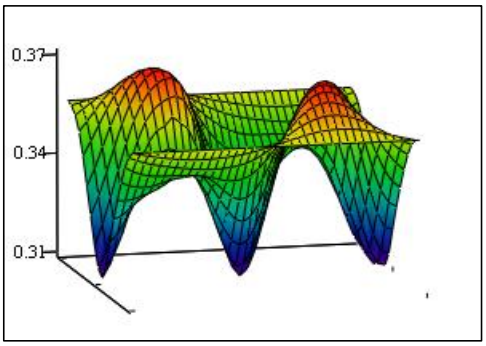

n

Fig. 7 Example of cross-pol coherence signature for forest in Bear Lakes area for 20060822-20061007

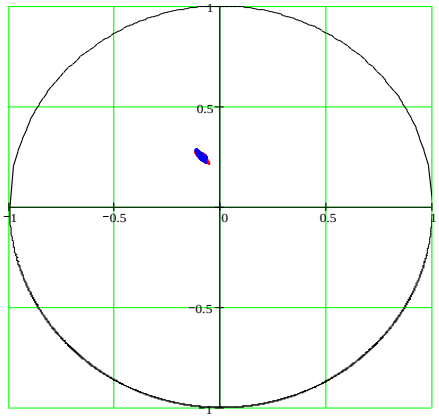

Fig. 8 Example of location of coherence on unit circle for forest in pair 20060822-20061007

One more approach to classification used here was based on estimation of various texture features of natural targets in a combination with fractal approach and applied to a set of the data collected over test site in Baikal area. It was shown that the use of fractal dimensionalities gives a possibility to describe the natural communities in exact quantitative way and provides the classification of earth covers. Three large classes with different values of fractal dimensionalities were classified: smooth homogeneous areas, rough fragments with a small bushes and forest stands.

The next direction of studies was analysis of temporal variations of forests scattering properties. Using a data set of 14 ALOS PALSAR quad-pol images of the eastern coast of the Baikal Lake (Siberia). In a given case study area included different types of land cover: two forests on flat land, mountainous forest, fields, meadows, waste grounds, the delta of the Selenga river (Baikal Lake coast, Siberia). Table 1 illustrates a seasonal distribution of observations dates, orbit (descending/ascending), air temperature, and precipitation (the last two parameters are from a meteo-archive at the website www.rp5.ru).

Table 1 Selenga quad-pol data takes parameters.

Date (yyyymmdd)	Orbit	Tempera-ture, °C	Precipi-tation
20060530	Descending	+9	rain
20060628	Ascending	+20	-
20060715	Descending	+13	-
20060813	Ascending	+10	rain
20060830	Descending	+10	-
20060928	Ascending	+7	-
20061015	Descending	-1	-
20061113	Ascending	-2	snow
20061130	Descending	-11	snow
20070331	Ascending	-1	-
20070516	Ascending	+9	-
20070602	Ascending	+5	rain
20071116	Ascending	-11	snow
20080402	Ascending	0	-

One can see in the table that in spite of the formal absence of winter observations the weather conditions demonstrate a sufficient variability, and without loss of generality the data set can be called a year-round imaging. Seven images cover a spring-and-summer vegetation period, when the growth is intensive, and surface changes are strongly pronounced.

A September image can be interpreted as early fall with +7°C air temperature, and two November dates demonstrate a winter type of whether with -11°C. During the rest four dates the temperature was negative near-zero. It is worth noting two outstanding weather details for 4 observation dates: 1) cyclonic frontal passage was attended by a heavy rain during the date 20060813; and 2) wet and packed snow cover on 20061015, 20070331, and 20080402 (snow surface for other winter-like dates is described like “dry snow”).

Eight regions of interest (ROI) were selected for analysis: three forests (coniferous and mixed ones on flat land, and pine forest in mountains), three fields in different places, and two patches of different backscatter level in between the delta network.

The study consisted of three independent parts and the subsequent comparison of their results. The first part was a plotting of a backscatter in three polarimetric channels for all eight regions. Mean intensities in HH, HV, VV polarizations were computed for each ROI and plotted as a function of a date. The second part was entropy/anisotropy/alpha classification by Cloude and Pottier for the whole time series. Mean values of all three parameters were calculated and compared. The third part of the data processing was classification by Freeman and Durden. A contribution of three scattering mechanisms (surface, volume and double-bounce) in the

total power was estimated for each date. For all 8 ROIs these dependences were graphed.

The most attractive part of the study was certainly an examination of plots of different polarimetric parameters for different types of cover, comparison of classification results, their correlation with weather conditions, and discussion of capabilities of the methods.

Plotting mean values of radar cross-section in co- and cross-polarized channels show that the backscatter level of forests decreases during freezing weather (see Fig. 9,10). HV polarization demonstrates a greater dip than co-polarized data. VV polarization plot looks like HH plot with slight difference, so it is not placed here. The difference in RCS for summer and winter-like dates reaches 8 dB in HH and VV polarizations, and 11 dB in HV polarization plot.

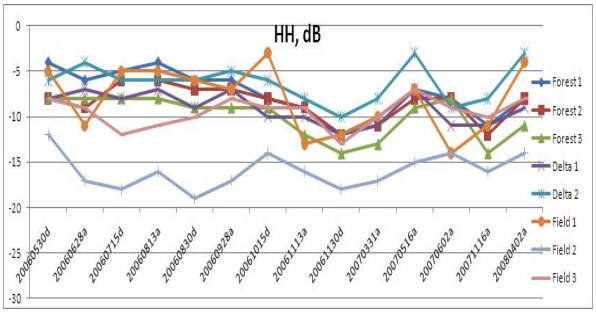

Fig. 9 RCS, HH polarization, for 8 regions of interest

Non-forested surfaces also show dips for two cold November dates (20061130 and 20071116), but their depth is in general less than forests' one. The whole graph for fields and delta patches have higher instability than forests. The reason is in vegetation volume changes and agricultural works in fields (e.g., harshness of the plot for *Field 1*). *Field 2* looks like very smooth surface with the lowest RCS values for all dates.

In Fig. 2 all three forests are above other graphs, two fields (*Field 1* and *2*) are below, and *Field 3* sometimes crosses two delta graphs.

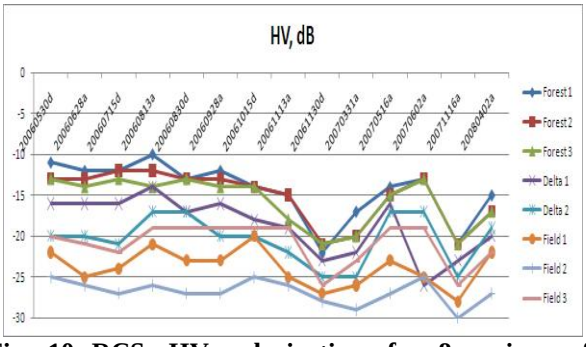

Fig. 10 RCS, HV polarization, for 8 regions of interest

So, in general, for all dates three types of the surface can be distinguished by their backscattering level in cross-polarization. The behavior of HH graphs is more entangled. Consequently we may use more advanced tools compared two simple backscatter level investigation.

The main point of this method consists in computing of three characteristics of coherency matrix. The entropy shows a degree of difference of its eigenvalues, the anisotropy marks the difference between two minor eigenvalues, and the alpha angle parameterizes weighted first coordinates of the eigenvectors. The values of α angle and entropy for all 14 dates are plotted on Fig. 11, 12, respectively.

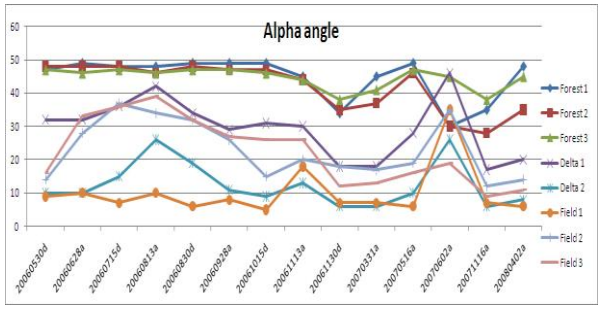

Fig. 11 Angle α, in degrees, for 8 regions of interest

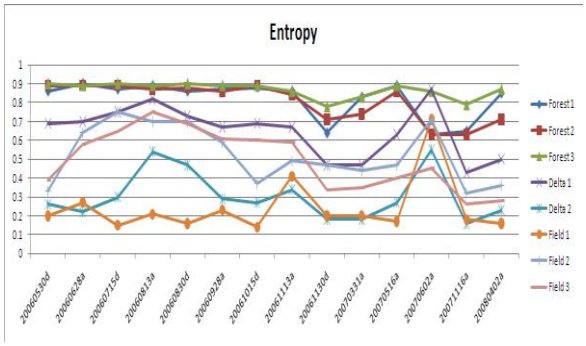

Fig. 12 Entropy, for 8 regions of interest

In contrast to Figures 9,10 three groups of graphs are clearly seen in Alpha and Entropy plots: the most stable three forests polylines are very close to each other, especially for the year 2006, three graphs (*Delta 1*, *Field 2* and *Field 3*) in the central band of the alpha and entropy plots, and two lowest polylines (*Field 1* and *Delta 2*). Two delta patches are naturally in different classes because of different level of backscattering and different type of vegetation (*Delta 1* includes some trees and little groves, but *Delta 2* is completely free of trees). The entropy of *Field 1* is the lowest for the major portion of observation dates. Probably the second delta patch has the surface scattering mechanism close enough to the *Field 1* to be in the same class with it. In general, five non-forested areas show significant variability of H, A and α values.

A freeze on 20061130 results in a fall of the alpha angle below 40°, and entropy value becomes lower than 0.8 (0.63 for *Forest 1*, 0.71 for *Forest 2*, and 0.78 for *Forest 3*). On 9-zone classification map the dipole and double-bounce classes vanish at this date and also for the second freezing day 20071116. Thus the moisture content of the trunks and brunches under freezing weather conditions is so low that the surface scattering mechanism becomes the absolute dominant even in forested areas. Non-forested areas have the entropy value below 0.5 and alpha angle below 20° for two frozen November dates that leads to placing them all in low-entropy surface scattering class. The same low values non-forested areas demonstrate also for March and April dates with air temperature -1°C and 0°C. Two

other days with negative temperature kept *Delta 1* and *Field 3* in usual medium-entropy surface scattering class. Four non-forested areas (*Fields 1,3, Deltas 1,2*) demonstrate the increasing alpha and entropy values for the date 20060813 with a heavy rain.
It is worth noting that unexpected peaks in Figures 11,12 on the date 20070602 are because of strong scene shift resulting in choose new ROIs for this date, and unfortunately they were found unsuitable.
This decomposition allows calculating the contribution of volume, surface and double-bounce scattering mechanism in the total power. On Fig. 13 one can see that the volume scattering (dashed line) dominates in forest, and that surface (dotted line) is the main scattering type in other ROIs.

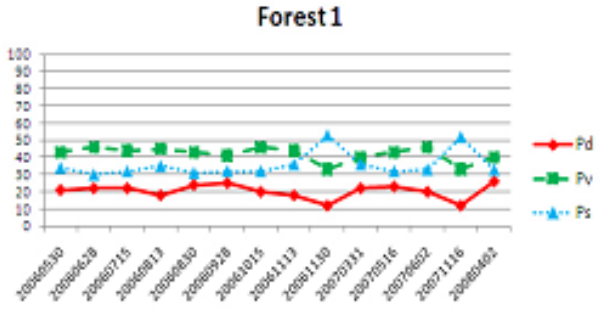

Fig. 13 Double-bounce (Pd), volume (Pv) and surface (Pv) scattering components (%), in forest

The *Forest 1* plot, for example, gives a nice emphasis of two freezing dates by two peaks of scattering component and simultaneous dips of volume and double-bounce (solid line) components.
Application of three polarimetric processing methods (three-channel analysis, Cloude–Pottier decomposition, Freeman–Durden decomposition) to the time series of PALSAR data shows an explicit dependence of scattering mechanisms for a given area on seasonal weather conditions. Winter freeze results in RCS decreasing for all polarization channels (1st method); and also in vanishing dipole and double-bounce scattering mechanisms and lowering of entropy and alpha values (2nd method); and also in significant increasing of surface scatter contribution (3rd method). Alpha-entropy method reveals the best capability for distinguishing different cover types for time series of polarimetric data. Freeman and Durden decomposition shows obviously the contribution of three types of scattering.
A compliance of both decompositions results confirms a reliability of conclusions, and additional details of each of them make a general picture more evident and complete.

3.3.2. Change detection.

Change detection is most impressive task as it allows the demonstration of the surface covers instability in various areas. A preference at this stage was paid to the areas of karst, landslide, soil subsidence, seismic activity areas as well as permafrost areas. These are:

- karst surfaces in proximity of railroad near Dzerzhinsk city,
- Volga riverbank in center of Ylyanovsk city with probable landslide activity,
- Yamburg-Nyda gas pipelines running in permafrost area, Western Siberia.
- Baikal-Amur railroad near Kazankan railway station with landslide activity,
- soil subsidence in Kemerovo underground coal mining area,
- landslide activity in Geyser valley, Kamchatka.
- tectonic activity in Baikal Lake area.

Classical DINSAR approach was used for a study, when 2-3 sessions were combined in interferometric set, flat topography was removed and the phase variations on the interferogram were attributed to surface dynamics. Most of the pairs had small spatial baseline, consequently the topography might be neglected.
It should be noted that most of these test sites were intensively studied by now with a use of ERS and ENVISAT data. C-band repeated orbits interferometry data were discovered to be practically useless because of temporal decorrelation.
PALSAR observations of Dzerzhinsk city area in 2007 provided nice datasets allowing clear indication of surfaces subsidence. The area is Dzerzhinsk are attractive for interferometric analysis because of high risk of permanent karst processes for the city's infrastructure and for Gor'koskaya railway. The basis of karst processes is the solution or leaching of fissured dissoluble rocks by underwater resulting in depression landform on the earth surface and different cavities, tunnels and caves under underground. Nizhny Novgorod region is famous for the dissoluble (karsting) rocks are carbonate rocks (limestone and dolomite) and sulphate ones (gypsum, anhydrite). In Dzerzhinsk area the territory is karsted by carbonate-sulphate karst and in some areas by gypsum karst. The typical karst phenomena are karst gaps, local subsidence and karst-piping slumps with probable low scale dynamics. Large amount of peatbogs in surroundings is of interest for the large-scale subsidence detection.On Figures 14 and 15 we present fragment of image and interferogram for a pair with 3 months separation obtained in FBD34.3 mode. We have to mention that similar bright patches generated by surface subsidence are seen on interferogram from a pair 20070705-20071005, which overlaps previous pair in time.
When processing two more PALSAR pairs – 20070705-20070820 and 20070820-20071005 we discovered that there are no any changes in the second pair, but all the surface displacements occurred between 20070705 and 20070820. So far, 3 pairs confirmed the fact of subsidence; all the subsidence occurred between 20070705 and 20070820. The nature of subsidence here according to topographic maps is soils drying in swamp areas. Karst processes were not detected because of significantly smaller size of karst zones.
Landslide activity was looked for with PALSAR data in urban area of Sochi city and area of railways running along the Black sea coast. No obvious dynamics was detected on relatively a short time intervals in summer 2007, as well as because of typically small landslide

zones in the area of study. But an impressive feature of PALSAR L-band data compared with C-band data is good coherence in such a vegetated area.

Fig. 14 Intensity image of karst area near Dzerzhink city from 20070618

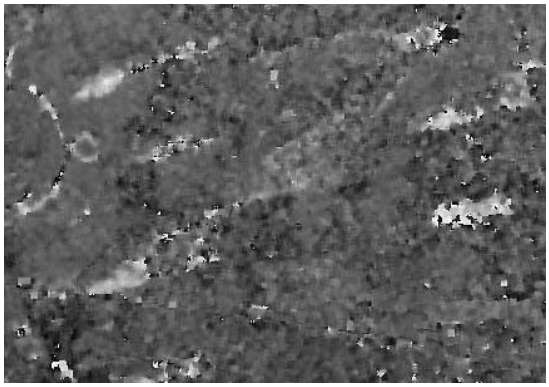

Fig.15 Interferogram of karst area near Dzerzhink city from pair 20070618-20070918

The same positive side of PALSAR is high coherence may be said according to our results in Ylyanovsk city riverbank area, using interferogram obtained in pair 20070805-20070920. Ulyanovsk is one of the important industrial and densely populated cities in Volga River region. It is situated at the cross of the waterway (Volga) from the north to the south and the arterial road London-–Vladivostok. Historically landslides of the right bank of the Volga River within the precincts of the city were frequent. The most destructive catastrophes of the last century in the city occurred in 1902, 1915, 1955, 1965. Nowadays local small landslides destroy up to 200 summer cottages every year. In the danger zone of 25 km length there are historical center of the city (mountain Venets), urban residential districts, service lines, power lines, roads. The most important geological causes of the landslides in the region are montmorillonite, which is one of the components of Volga riverbanks, undercutting of the bank slopes by the river, and steep slopes. Therefore the most dangerous season is the spring with rains, snow melting and high water. Water makes montmorillonite swell, and this fact causes a deformation of geological layers. Water layers became stronger after rains, and they play a part of slickensides.

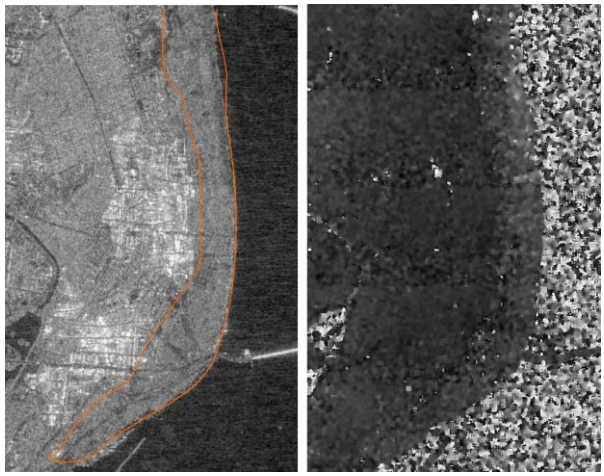

Fig.16 PALSAR image (left) and interferogram (right) of Ulyanovsk city, pair 20070805-20070920

Very short spatial baseline (50 meters perpendicular component, when 360^0 phase variations require 1200 m topography variations) allowed us to suppose small – scale sliding of riverbank soil between the observations (see Fig. 16). Another impressive preference of L-band PALSAR data was the fact the coherence exists in the pair of data obtained on winter as well as for autumn-winter period, what is not a case with C–band data.

On the next Figures 17 and 18 below winter pair of Yamburg-Nyda gas pipeline location with 45 days repeat interval from another study is presented.

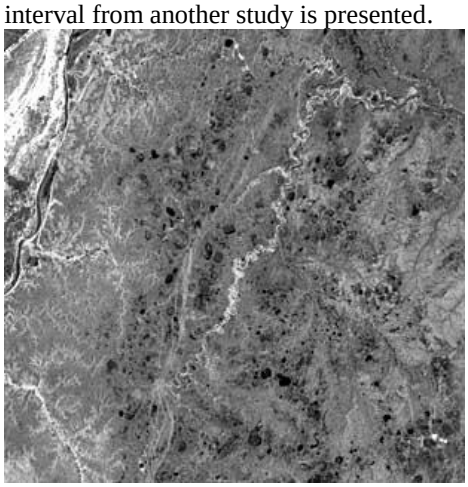

Fig. 17 Intensity image from 20070113 (entire scene)

Positive fact is remarkably high coherence everywhere in winter pair, though some areas – 4 horizontal diffuse stripes – show decrease of coherence. Very possible explanation of the phenomenon is that we observe here corrupting influence of ionosphere fluctuations during one of the observations. Large-scale ionosphere gradients in disturbed ionosphere (ionosphere streaks, which are frequent in winter at high latitudes) caused local displacements of the image fragments within the synthesized image, for that reason the coregistration quality was varying across the SAR scene. It should be noted here that this effect was observed only on this interferogram, though many PALSAR interferometric datasets for other regions were processed by now.

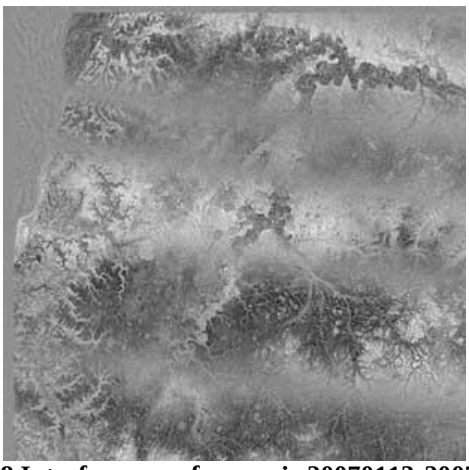

Fig. 18 Interferogram from pair 20070113-20070228

Among the corrupting effects in this area were seasonal displacements of soils surface because of soil watering/drying processes.

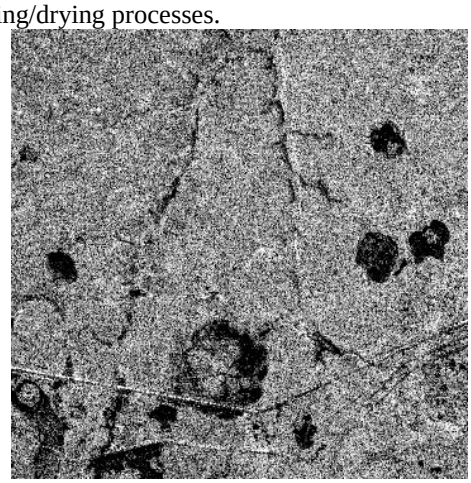

Fig. 19 Amplitude image from 20100608

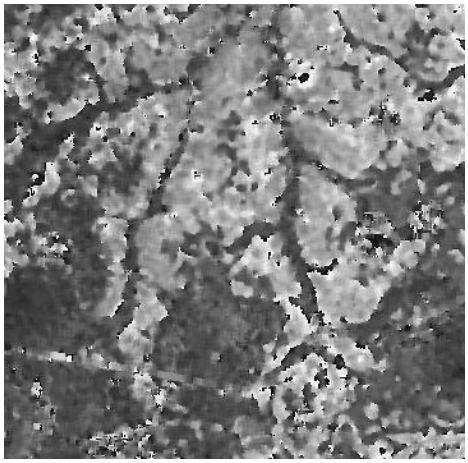

Fig. 20 Interferogram from pair 20100608-2010724

One of the effects we were looking for is demonstrated on the next figure. Image fragment with a pipe running in horizontal direction is accompanied with an example of the gas pipe displacement in permafrost area is seen on the interferogram in brighter tones.

The form of displacement is surface subsidence because of soils drying/permafrost thawing in the end of summer – mid of autumn, warm and dry period for this area. Other interferometric pairs obtained in autumn demonstrate pipes uplift because of permafrost heave in other areas of study (Fig. 21, 22).

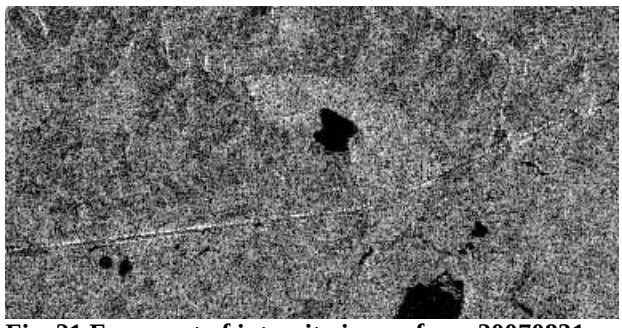

Fig. 21 Fragment of intensity image from 20070831

Fig. 22 Interferogram from pair 20070831-20071016

The next demonstration of PALSAR interferometry application is monitoring the landslide activity in the vicinity of Baikal-Amur railroad near Kazankan railway station. The railroad near Kazankan station was constructed in a complicated seaismoactive area on the hill slope. During the 10 years of the road functioning a number of slides occurred damaging the railroad permanent way.

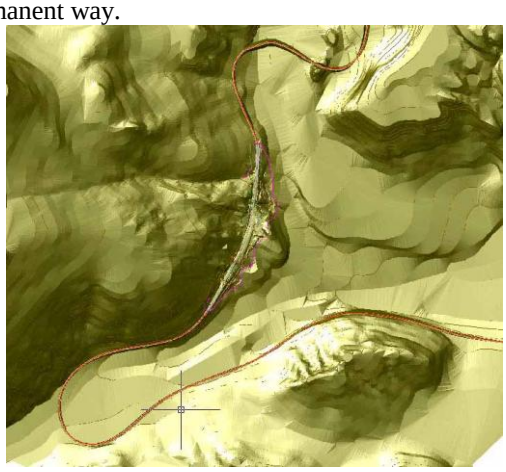

Fig. 23 DEM of the area of railway location

On the amplitude image on a Fig. 24 the arrows show the location of railway bridges over the riverbeds with high potential of landslide activity. On the differential interferogram for a pair 20070112-20090117 on the Fig. 25 the arrows mark dark spots corresponding to the landslides detected with this technique.

Soil subsidence in the Kemerovo underground coal mining area, from a next study, was reliably detected in summer 2007 and 2010 on a series of interferometry pairs. The area of coal mining activity is famous for its frequent earthquakes in the areas of underground coal

excavation. On the Fig. 26 amplitude image and interferogram from summer 2010 is presented.

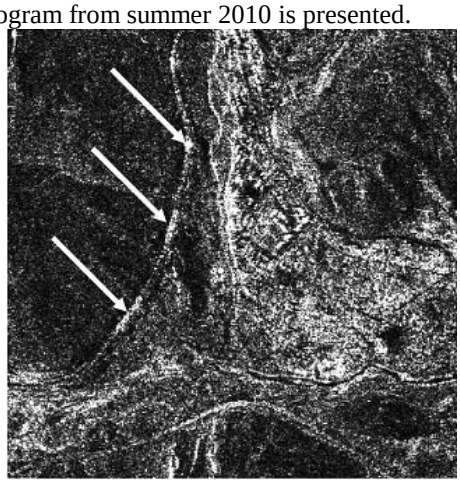

Fig. 24 PALSAR image of railway near Kazankan

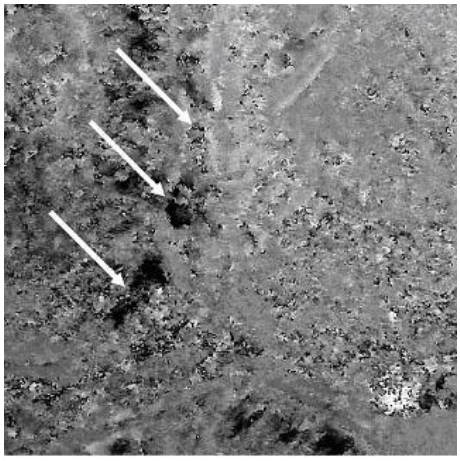

Fig. 25 PALSAR interferogram of landslide area near Kazankan railway station

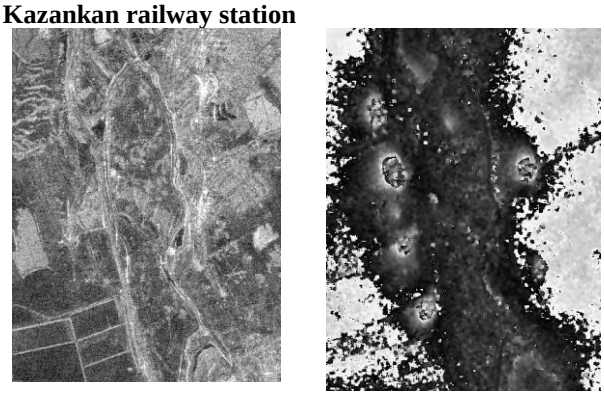

Fig.26 Amplitude image and interferogram of coal mining area in summer 2010

Clear fringe patterns on the interferogram correspond to the location of coal mines and show 10-13 cm subsidence of the soil over the mines. Typical size of subsiding area is 300-500 m. Dense seismometer network in the area allowing the detection of earthquakes location shows tight interconnection of the places of subsidence with earthquakes. On the Fig. 27 3D representation of the soil subsidences is given.

A series of interferograms for other dates were also created using PALSAR data. On the Fig. 28 two adjacent interferograms from summer 2007 are presented.

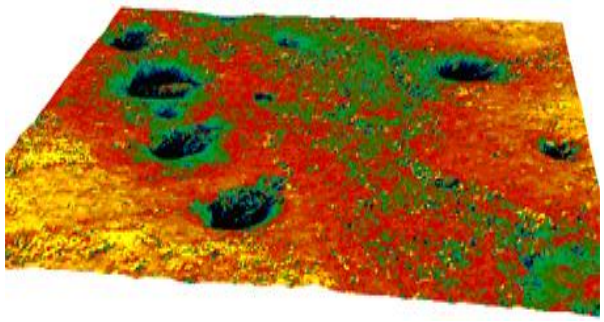

Fig. 27 3D representation of subsidence in Kemerovo coal mining area in summer 2010

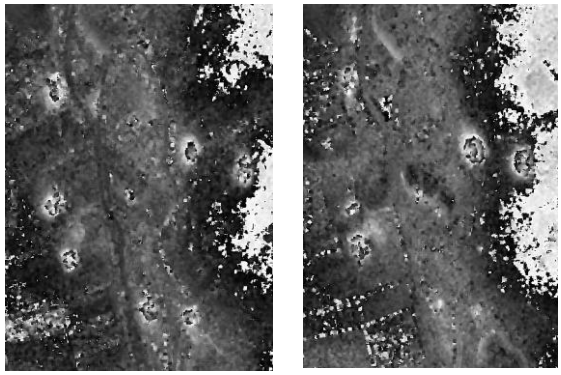

Fig. 28 Two adjacent interferograms of coal mining area in summer 2007

One can see here that the location and amplitude of subsidence over coal mines is varying with time.

The area of one more study is Kamchatka Peninsula with frequent earthquakes, landslides and volcanic eruptions. On the next figure amplitude images of landslide area near Geyser Valley are presented. The landslide happened on June 07, 2007 covered with soil prominent part of this natural heritage.

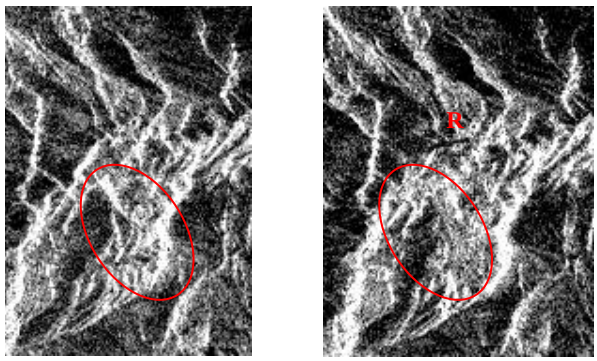

Fig. 29 Two amplitude images of landslide (before and after event) in Geyser Valley, Kamchatka.

Red ellipse marks the location of landslide on the images above. Letter R on the right image marks the location of pond (dark horizontal line) after the small river in Geyser Valley was partitioned. As the landslide activity is still going on in Geyser Valley, what leads to temporal decorrelation of signals scattered from landslide body. For that reason interferometry techniques for a change detection studies are not applicable here.

Most of surface dynamics effects in a given project were detected in Selenga delta area, one of calibration sites.

The area is famous for frequent earthquakes with large magnitude. On the Fig. 30 a map of the area with location of active breaks marked with yellow color is presented. Signs of seismic activity were discovered in form of centimeter displacements of land along the known fault on the beach on the PALSAR pair form January 2007- February 2009.

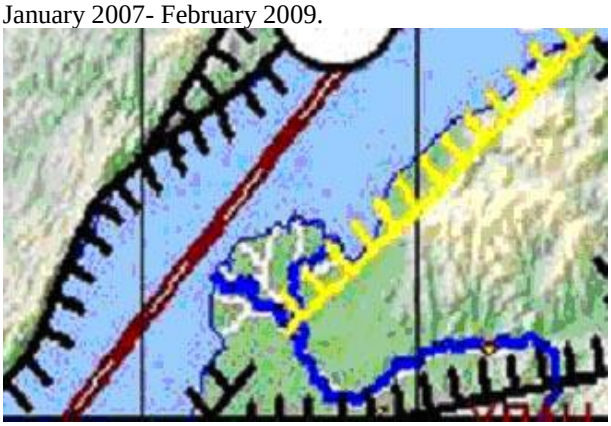

Fig. 30 Map of the Selenga river delta with location of active break

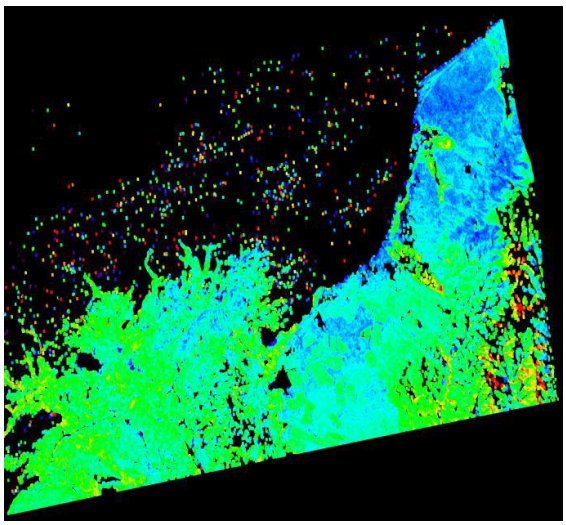

Fig. 31 Color-coded differential interferogram of Selenga river delta area for a period 2007-2009

Among other effects detected here was soil heaving in the area of paleoriverbed, which was detected on January 2009-February 2009 interferogram. Georadar studies of soils in this area in winter 2009 confirmed the subsoil water freezing as a source of local surface uplift.

4. CONCLUSION

Four years of calibration activities with PALSAR have shown that calibration antennas of Bear Lakes test site may be used as calibration targets in L-band for analysis of radiometric stability. Natural strong scatterers may be found within the scene as candidates for calibration in addition to artificial targets. In calibration experiments with PALSAR we discovered that overall PALSAR + calibration targets radiometric stability is about 0.54 dB according to measurements of strong natural scatterer. Radiometric stability in the measurements of reflector antennas was found to be somewhat lower – 0.64 dB for most stable antenna, probably because of influence of pointing errors.

New technique, the coherence signatures technique, was proposed and tested using polarimetric datasets for Moscow region and Baikal region. New classification approaches like as textural and/or fractal analysis applied to SAR data are tested on Istomino test site.

Application of three polarimetric processing methods (three-channel analysis, Cloude–Pottier decomposition, Freeman–Durden decomposition) to the time series of quad-pol PALSAR data demonstrated an explicit dependence of scattering mechanisms for a given area on seasonal weather conditions.

Interferometry technique was fruitful also in the detection of surface dynamics in many Russian test sites.

5. REFERENCES

[1] A.I. Zakharov. “Separate Estimation of Faraday Rotation and Topography Effects from Polarimetric SAR Data.” Proc. 6th European Conference on Synthetic Aperture Radar, Dresden, Germany, 2006

[2] A.I. Zakharov et al, "First results of Japanese PALSAR calibration by means of OKB MEI calibration test site", Proceedings of 4th All-Russian conference “Modern problems of Earth remote sensing from Space”, Moscow, Russia, 2006.

[3] A.I. Zakharov, "Seasonal variations of Earth sounding media polarimetric properties using first PALSAR data", Abstract book of the 3rd International Workshop POLINSAR-2007, Frascati, Italy, 2007.

[4] L.N. Zakharova, "Land cover classification based on polarimetric coherence signatures ", Abstract book of the 3rd International Workshop POLINSAR-2007, Frascati, Italy, 2007.

[5] L.N. Zakharova, "Classification of Earth covers by means of polarimetric interferometry technique applied to SAR data", Proceedings of XXV Symposium on radar sensing of natural covers”, Saint-Petersburg, Russia, 2007.

[6] L.N. Zakharova, "New technique of fully polarimetric SAR data analysis in repeated orbits interferometry scheme", Proceedings of XIII International conference , Voronezh, Russia, 2007.

[7] L.N. Zakharova “Forest classification by means of two POLINSAR techniques.” Proc. of 5th International Symposium BioGeoSAR-2007, Bari, Italy, 2007.

[8] L.N. Zakharova, «Exploitation of interferometric coherence generated from fully polarimetric SAR data for classification of Earth covers» Proceedings of 5th All-Russian conference “Modern problems of Earth remote sensing from Space”, Moscow, Russia, 2007.

[9] A.I. Zakharov et al, «Results of first year calibration of Japanese PALSAR SAR», Proceedings of 5th All-Russian conference “Modern problems of Earth remote sensing from Space”, Moscow, Russia, 2007.

[10] A.I. Zakharov, P.A. Zherdev and A.B. Sokolov, “PALSAR calibration with passive antenna reflectors”, *Abstract book of ALOS PI Symposium*, Greece, 2008.

[11] A.I. Zakharov, L.N. Zakharova, “PALSAR change detection in urban areas of European part of Russia”, *Abstract book of ALOS PI Symposium*, Greece, 2008.